ADVANCED FUNCTIONAL MATERIALS
www.afm-journal.de

Materials Views
www.MaterialsViews.com

Effectively Utilizing NIR Light Using Direct Electron Injection from Up-Conversion Nanoparticles to the TiO_2 Photoanode in Dye-Sensitized Solar Cells

Jie Chang, Yanhui Ning, Suli Wu, Wenbin Niu, and Shufen Zhang*

TiO_2/$NaYF_4$:Yb^{3+},Er^{3+} nano-heterostructures are prepared in situ on the TiO_2 photoanode of dye-sensitized solar cells (DSCs). Transmission electron microscopy (TEM) and high-resolution (HR)-TEM confirm the formation of TiO_2/$NaYF_4$:Yb^{3+},Er^{3+} nano-heterostructures. The up-converted fluorescence spectrum of the photoanode containing the nano-heterostructure confirms electron injection from $NaYF_4$:Yb^{3+},Er^{3+} to the condution band (CB) of TiO_2. When using a photoanode containing the nano-heterostructure in a DSC, the overall efficiency (η) of the device is 17% higher than that of a device without the up-conversion nanoparticles (UCNPs) and 13% higher than that of a device containing mixed TiO_2 and UCNPs. Nano-heterostructures of TiO_2/$NaYF_4$:Yb^{3+},Tm^{3+} and TiO_2/$NaYF_4$:Yb^{3+},Ho^{3+} can also be prepared in situ on TiO_2 photoanodes. The overall efficiency of the device containing TiO_2/$NaYF_4$:Yb^{3+},Ho^{3+} nano-heterostructures is 15% higher than the control device without UCNPs. When nano-heterostructures of TiO_2/$NaYF_4$:Yb^{3+},Tm^{3+} are used, the open-circuit voltage (V_{oc}) and the short-circuit current density (J_{sc}) are all slightly decreased. The effect of the different UCNPs results from the different energy levels of Er^{3+}, Tm^{3+}, and Ho^{3+}. These results demonstrate that utilizing the UCNPs with the apporpriate energy levels can lead to effective electron injection from the UCNPs to the CB of TiO_2, effectively improving the photocurrent and overall efficiency of DSCs while using NIR light.

1. Introduction

Considerable scientific and industrial attention has been focused on dye-sensitized solar cells (DSCs) over the past two decades because of their low cost, environmental friendliness, and simple preparation procedures for various photovoltaic devices.[1] One focus of current research is to further increase the energy conversion efficiency of DSCs.[2,3] The sensitizers that are typically used include heteroleptic ruthenium (Ru) complexes[4] and organic dyes;[5,6] they only absorb sunlight in the visible region. Meanwhile, the infrared and near-infrared (NIR) spectral parts of sunlight, which comprise almost half of the energy of the sun's radiation, have not been utilized by these sensitizer. Consequently utilizing the infrared and NIR parts of sunlight has become an important target for increasing the energy conversion efficiency of DSCs.

One strategy for utilizing NIR light was to develop panchromatic sensitizers, but the poor electron injection efficiency and competing charge recombination of the NIR sensitizers hampered their development.[7] An alternative approach for improving light-harvesting in the NIR region was the utilization of up-conversion nanoparticles (UCNPs), which transform NIR light (>800 nm) into visible light (<750 nm).[8–10] Recently, β-$NaYF_4$:Yb^{3+},Er^{3+} hexagonal nanoplatelets and $Y_3Al_5O_{12}$:Er^{3+},Yb^{3+} were attached at the rear (external) of adye-sensitized solar cell; they could simultaneously reflect light and make use of NIR light.[11,12] Additionally, a TiO_2/UCNP (made of Er^{3+}/Yb^{3+}-doped LaF_3) nanocomposite was used as an internal component of a DSC to enhance light-harvesting in the NIR region.[13] This work however proved ineffective in delivering a higher photocurrent output because of apparent charge recombination at the UCNP/dye/electrolyte interfaces. Khan et al. and Xie et al. also reported a photocurrent decrease and photovoltage increase in UCNP-integrated dye-sensitized solar cells.[14,15] In addition, colloidal up-conversion nanocrystals were explored for DSCs. The utilization of colloidal UC nanocrystals was found to enhance the photocurrent of the cells under infrared irradiation, while the overall conversion efficiency of the cells including UC nanocrystals (2.8%) is only slightly higher than that of the cell without UC nanocrystals (2.7%).[16]

All of the above-mentioned research focused on two aspects: i) the conversion of NIR light to visible light by UCNPs and how the converted visible light was absorbed by the dye-sensitizer (radiatively or nonradiatively), and ii) the reflection of light. Due to the low emission efficiency of UCNPs, the large energy lose during radiative or nonradiative energy transfer from the UCNPs to the dye sensitizer, and the apparent charge recombination at the UC/dye/electrolyte interfaces, it is difficult to achieve a higher photocurrent output and overall efficiency. The

Dr. J. Chang, Y. Ning, Prof. S. Wu, Dr. W. Niu, Prof. S. Zhang
State Key Laboratory of Fine Chemicals
Dalian University of Technology (DUT)
Dalian, 116024, China
E-mail: wusuli@dlut.edu.cn

DOI: 10.1002/adfm.201301158

UCNPs can absorb low-energy photons (>800 nm) and produce excited electrons located at high energy levels (<750 nm) by a multi-photoprocess. If the excited electron in the high energy level of UCNPs can directly be injected into the conductive band (CB) of TiO_2 and the oxidized UCNPs can be reduced by the redox couple (I_3^-/I^-) like the working process of the dye-sensitizer in DSCs, the doping of UCNPs that are incorporated into DSCs will effectively improve the photocurrent and overall efficiency of the DSCs.

In nano-heterostructures containing two or more nanoscale components, the shared interfaces in hybrid nanoparticles facilitate charge-, energy-, and spin-transfer between different components.[17] Our previous work and that of others have indicated the possibility of electron transfer from UCNPs to quantum dots (QDs) in UCNP/QD nano-heterostructures.[18] In order to realize electron transfer from UCNPs to the CB of TiO_2, the in situ preparation of TiO_2/UCNP nano-heterostructures on TiO_2 photoanodes is demonstrated in this work. β-$NaYF_4$:Yb^{3+},Er^{3+}—one of the effective up-converter materials—was selected for the formation of nano-heterostructures because its energy levels match the CB of TiO_2 well. The TiO_2/β-$NaYF_4$:Yb^{3+},Er^{3+} nano-heterostructures were incorporated into DSCs, and they were shown to effectively enhance the photocurrent and overall conversion efficiency of the DSCs by 9.5% and 17.5%, respectively.

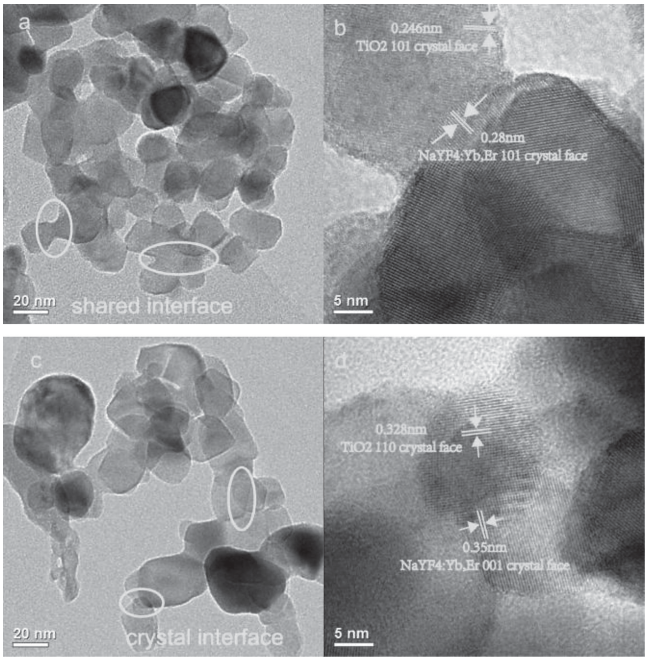

Figure 1. a,c) TEM (a,c) and b,d) HR-TEM images of TiO_2/UCNP nanocomposites sintered at a,b) 450 and c,d) 400 °C.

2. Results and Discussion

The size of the TiO_2 nanocrystals typically used in DSCs is about 10–20 nm, and they are usually produced by a hydrothermal synthesis. Aimed at forming nano-heterostructures and effectively inject electrons into TiO_2, β-$NaYF_4$:Er^{3+},Yb^{3+} nanoparticles of relatively smaller size and high emission intensity were synthesized using an improved hydrothermal method (see Experimental Section). The average particle size of the as-prepared UCNPs was about 40–50 nm (Figure S1, Supporting Information). From the X-ray diffraction (XRD) patterns, we observed that the peak positions and intensities of all the samples agreed well with the calculated pattern for hexagonal $NaYF_4$:Yb^{3+},Er^{3+} crystals (Joint Committee for Powder Diffraction Standards, JCPDS No. 16-0334), and impurities were not detected. For comparison, β-$NaYF_4$:Yb^{3+},Er^{3+} was also synthesized by the traditional method (see Supporting Information).

The up-conversion fluorescence spectra of $NaYF_4$:Yb^{3+},Er^{3+} prepared by the improved synthetic and the traditional methods are obtained for samples measured under the same conditions (Figure S2, Supporting Information). The green and red emission bands at about 524, 540, and 660 nm were clearly observed, and they were assigned to the $^2H_{11/2}$–$^4I_{15/2}$, $^4S_{3/2}$–$^4I1_{5/2}$, and $^4F_{9/2}$–$^4I_{15/2}$ transitions, respectively, of the Er^{3+} ion. Clearly, the emission intensity of $NaYF_4$:Yb^{3+},Er^{3+} prepared by the improved synthetic method was significantly higher than that of samples prepared by the traditional hydrothermal method. In the following, UCNPs prepared by the improved synthetic method were used.

The prepared UCNPs were mixed with TiO_2 (at a UCNP:TiO_2 ratio of 15:85) in a solution of ethylcellulose in terpineol (10%) to form a paste. The pastes were screen-printed onto glass and sintered at 400 °C (composite film A) or 450 °C (composite film B) in air for 0.5 h. The sintered products were re-dispersed in ethanol and characterized by transmission electron microscopy (TEM) and high-resolution (HR)-TEM. As **Figure 1** shows, after sintering at 450 °C, some crystal interfaces (as indicated in Figure 1a) between TiO_2 and the UCNPs disappeared and shared interfaces were formed. The HR-TEM image reveals an interlayer spacing of 0.246 nm in a single nanoparticle, in good agreement with the *d* spacing of the (101) lattice plane of TiO_2 (Figure 1b). In the other nanoparticle,, the interlayer spacing of 0.28 nm is observed; this agrees with the lattice spacing of the (101) plane of Yb^{3+},Er^{3+}. The two nanoparticles share an interface, which confirms the formation of TiO_2/UCNP nano-heterostructures. In samples sintered at 400 °C, a clear interface still existed (Figure 1c), indicating that the TiO_2 and UCNPs were only physically mixed, and no nano-heterostructures had formed. The HR-TEM image also indicated that $NaYF_4$:Yb^{3+},Er^{3+} and TiO_2 have a clear interface after being sintered at 400 °C.

To prove electrons can be injected from the UCNPs to TiO_2 in the nano-heterostructure, the room-temperature up-conversion fluorescence spectra of TiO_2/UCNP were obtained after an excitation at 980 nm for composite film A, composite film B, and a UCNP film without TiO_2 (before and after sintering at 450 °C in air for 0.5 h), as shown in **Figure 2**. For the film A, strong green and red emission bands at about 524, 540, and 660 nm were all clearly observed similar to that of the UCNP film. For film B however, green emissions at 524 and 540 nm nearly disappeared. Because the up-conversion fluorescence spectrum of the UCNP film without TiO_2 that was sintered at 450 °C was very similiar with that of the UCNP film before calcination, the disappearance of the green emission bands of film B could not have been induced by calcination. The XRD patterns of film B were also obtained. As illustrated in the Supporting Information (Figure S3), the peak positions and intensities of

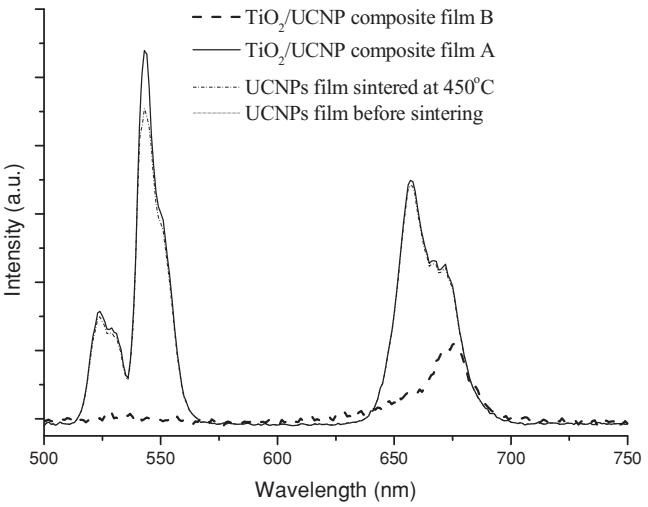

Figure 2. Up-conversion fluorescence spectra of TiO_2/UCNPs composite film A (sintered at 400 °C), TiO_2/UCNPs film B (sintered at 450 °C) and UCNPs film before and after sintered at 450 °C excited at 980 nm.

film B correspond to strong peaks of the standard pattern of the hexagonal $NaYF_4$:Yb^{3+},Er^{3+} crystal (JCPDS No. 16-0334) and TiO_2; impurities were not detected. Because the concentration of $NaYF_4$:Yb^{3+},Er^{3+} was only at 15%, the XRD patterns showed only the strong peaks of $NaYF_4$:Yb^{3+},Er^{3+}; the weak peaks could not be clearly observed. It was concluded that the disappearance of the green emission bands in film B was not caused by the structure and phase change of $NaYF_4$:Yb^{3+},Er^{3+}. These results suggested that in film B, the excited electrons located at the green emission level ($^2H_{11/2}$–$^4I_{15/2}$, $^4S_{3/2}$–$^4I1_{5/2}$) of hexagonal $NaYF_4$:Yb^{3+},Er^{3+} were quenched via a nonrelaxation path. According to the energy levels of $NaYF_4$:Yb^{3+},Er^{3+}, TiO_2 and the energy level of the redox couple (I_3^-/I^-; **Figure 3**A), the green emission level of $NaYF_4$:Yb^{3+},Er^{3+} is higher than the CB of TiO_2, and its ground state is lower than the energy level of the redox couple. This meets the conditions of electron injection from $NaYF_4$:Yb^{3+},Er^{3+} to the CB of TiO_2 and the reduction of the oxidized $NaYF_4$:Yb^{3+},Er^{3+} by the redox couple (I_3^-/I^-). Therefore it was assumed that the disappearance of the green emission bands was due to electron injection from $NaYF_4$:Yb^{3+},Er^{3+} to the CB of TiO_2. In film A, with the same components but calcined at 400 °C, an intense green emission is still present, indicating that the electron injection from $NaYF_4$:Yb^{3+},Er^{3+} to the CB of TiO_2 did not occur because no nano-heterostructure was formed; this is consistent with the results of TEM and HR-TEM. As Figure 3B illustrates, the shared interface in the nano-heterostructure facilitates electron injection from $NaYF_4$:Yb^{3+},Er^{3+} to the CB of TiO_2, while the crystal interface in the simply mixed composite hinders electron transfer.

To further confirm that the significant decrease of the green emissions of $NaYF_4$:Yb^{3+},Er^{3+} in film B was induced by electron injection from the UCNPs to the CB of TiO_2, film C composed of Al_2O_3 and UCNPs was prepared for comparisons. The up-conversion fluorescence spectrum of film C calcined at 450 °C (Figure S4, Supporting Information) illustrated that the emission changed little after calcination at 450 °C because of the difference between the energy levels of the UCNPs and CB of Al_2O_3. Although the higher temperature may further enhance the charge-transport ability, the high temperature will decrease the emission intensity of $NaYF_4$:Yb^{3+},Er^{3+}. We have investigated the up-conversion luminescence of $NaYF_4$:Yb^{3+},Er^{3+} after calcination at different temperatures. As Figure 2 shows, the up-conversion fluorescence spectrum of UCNPs sintered at 450 °C was very similar with that of UCNPs before calcination. However, when the calcination temperature is up at 500 °C, the luminescence intensity of $NaYF_4$:Yb^{3+},Er^{3+} decreased greatly (Figure S5, Supporting Information). As a result, we selected a calcination temperature of 450 °C.

DSC photoanodes with TiO_2/UCNPs nano-heterostructures, a mixture of TiO_2 and UCNPs, or only TiO_2 were prepared using screen-printing pastes based on the synthesized TiO_2–UCNPs nanocomposites and control TiO_2 (P25) nanoparticles produced via Grätzel's method.[19,20] Photoanode 1 comprised four layers of transparent TiO_2 made with P25 (about 16 μm thickness) and one layer of TiO_2–UCNPs nanocomposites (about 4 μm) thickness; it was sintered at 450 °C for 0.5 h in air. Photoanode 2 with the same components as photoanode 1 was calcined at 400 °C. The control photoanode consisted of four layers of transparent TiO_2 (photoanode 3, about 16 μm thickness) or five layers of transparent TiO_2 (photoanode 4, about 20 μm thickness) made with P25. The prepared control electrodes were calcined at 450 °C for 0.5 h in air. Then the photoanodes were sensitized by immersion in a 0.05 mM N719 dye (Dyesol)–ethanol solution. In order to optimize the structure of the (TiO_2–UCNP)-modified working electrode, the responding solar cell devices were assembled and tested.

According to the assumption that the electron can be injected from $NaYF_4$:Yb^{3+},Er^{3+} to the CB of TiO_2, the insertion of the TiO_2/UCNP nano-heterostructures layer in the photoanode should increase the photocurrent and overall efficiency of the DSCs. **Figure 4** shows the photocurrent–voltage curves of the four DSCs using photoanodes 1–4 under AM1.5 G sun. As **Table 1** illustrates, the control devices with photoanodes 3 and 4 exhibited overall efficiencies (η) of 3.55% and 3.32%, respectively, indicating that adding a layer of TiO_2 on photoanode 3 did not increase the overall efficiency of DSC. The open-circuit voltage (V_{oc}) and the short-circuit current density (J_{sc}) of the control device with photoanode 3 were 0.736 V and 8.65 mA·cm^{-2}, respectively. For the device with photoanode 1 incorporating the TiO_2/UCNP nano-heterostructures, the V_{oc} and the J_{sc} were increased to 0.765 V and 9.47 mA·cm^{-2}, respectively, and η reached 4.17%, which was 17% higher than that of the device without UCNPs (photoanode 3), thus highlighting the effect of electron injection from UCNP to the CB of TiO_2. As for the device with photoanode 2, although the UCNPs and TiO_2 were both present, the V_{oc} and J_{sc} values were close to those of the control device with photoanode 3 because nano-heterostructure were absent. This is consistent with the up-conversion spectra of the photoanodes. Absence of electron transfer led to no obvious enhancement in the efficiency. All these results demonstrate that the electron injection from $NaYF_4$:Yb^{3+},Er^{3+} to the CB of TiO_2 in nano-heterostructure play a key role in improving the overall efficiency of DSCs. **Scheme 1** illustrates the structure and function of the insertion of a layer of TiO_2/UCNP nano-heterostructures in the electrode structure.

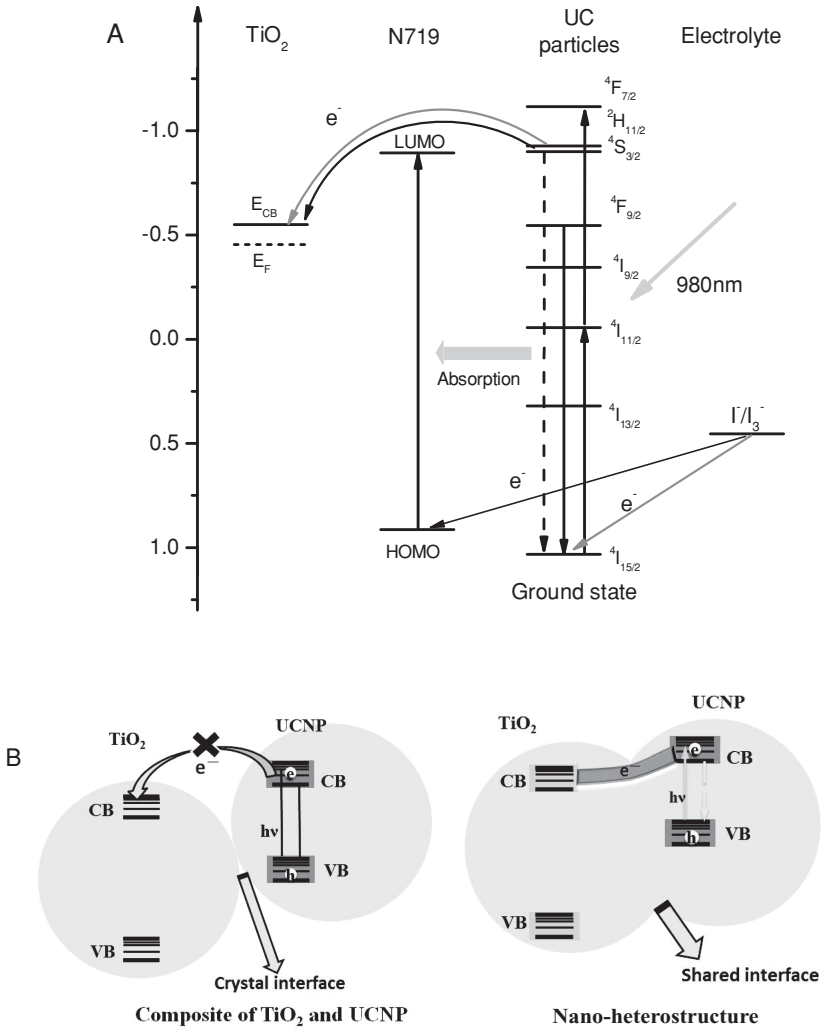

Figure 3. A) Energy level diagram of the UCNPs, N719 dye, and TiO_2, and the energy level of the redox couple (I_3^-/I^-), showing the electron transfer from the UCNPs to the CB of TiO_2, I_3^-/I^- to the ground state of the UC nanocrystals, and energy transfer from the UC nanocrystals to the N719 dye under irradiation with NIR light. LUMO = lowest unoccupied molecular orbital. HOMO = highest occupied molecular orbital. E_{CB} = energy of the condution band of TiO_2. E_F = Fermi level. B) Schematic representation of the composite and nano-heterostructure of TiO_2 and UCNPs. CB = conduction band. VB = valence band.

Compared with the literature,[13–16] using UCNPs and TiO_2 nanocomposites as an internal part of the DSC structure proved ineffective to enhance photocurrent output and overall efficiency because of apparent charge recombination at the UC/dye/electrolyte interfaces. Here, because of direct electron injection from the UCNPs to TiO_2, the insertion of the TiO_2/UCNP nano-heterostructures layer into the electrode structure effectively enhances the photocurrent and overall conversion efficiency of the DSCs by 9.5% and 17.5%, respectively.

To investigate the effect of the ratios of TiO_2 and $NaYF_4$:Yb^{3+},Er^{3+} on the DSC performance, different ratios were used to prepare photoanodes, and the performance of the resulting DSCs were measured. When the (TiO_2):($NaYF_4$:Yb^{3+},Er^{3+}) ratio was 85:15 (Table S1, Supporting Information), the device has the highest J_{sc} and overall efficiency (η).

It was reported that the suspended UC nanoparticles can also be regarded as scattering centers that increase the light absorbance of the film and lead to an efficiency increment of the solar cell.[21] Aiming to prove that the reason behind the efficiency increment in the work was electron injection rather than light scattering, $NaYF_4$ without doping was prepared under the similar conditions as that of UCNP. The obtained products were of similar size and morphology as UCNPs, but they cannot absorb NIR light and they cannot produce excited electrons at high energy levels because they do not contain any rare earth ions. They were also used to prepare photoanodes using the same preparation method as photoanode 1. The photocurrent–voltage curves (Figure S6, Supporting Information) showed that its V_{oc}, J_{sc}, and overall efficiency were all slightly lower than those of the control device. This may be taken as an indication that the efficiency increment was not caused by light scattering.

In order to improve unequivocally that the use of UCNPs indeed leads to photocurrent generation via the electron injection from UCNPs to the CB of TiO_2, the photocurrent–voltage curve using naked photoanode 1 and 2 without dyes was measured under AM1.5 G sun. A V_{oc} of 0.33 V and a J_{sc} of 0.085 mA were obtained under the AM1.5 G sun illumination (Figure S7, Supporting Information); even TiO_2 was not sensitized by the dye. Because dye was not used, the photocurrent generation did not result from the light absorption and electron injection of the dye into TiO_2. In addition, the emission of UCNPs cannot be absorbed by TiO_2 because their absorption and emission spectra are mismatched. This confirms the electron transfer from UCNPs to TiO_2.

The incident-photon-to-current efficiency (IPCE) and the dye loadings of photoanode 1 and 3 were measured. Generally, a higher dye loading in the photoanodes leads to a higher photocurrent density. The photoanodes with and without UCNPs showed similiar dye loadings, which indicated that the photocurrent enhancement of photoanode 1 was not induced by higher dye loading (Table S3, Supporting Information). As can be seen in the IPCE spectra (Figure S8, Supporting Information), the photon-to-current conversion efficiency of the photoanode with UCNPs was very close to that of the control photoanode, but it was obviously increaseed in the NIR region, indicating that the absorption of NIR light by the UCNPs was responsible for the current increase.

Nano-heterostructures of TiO_2/$NaYF_4$:Yb^{3+},Tm^{3+} and TiO_2/$NaYF_4$:Yb^{3+},Ho^{3+} were also prepared in situ on TiO_2 photoanodes. Figure S9 (Supporting Information) shows the photocurrent–voltage curves of the DSCs using the above

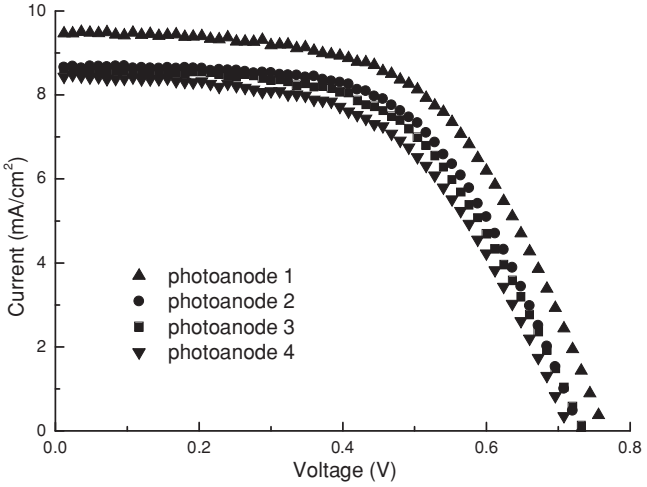

Figure 4. Photocurrent–voltage curves of DSCs with the different photoanodes.

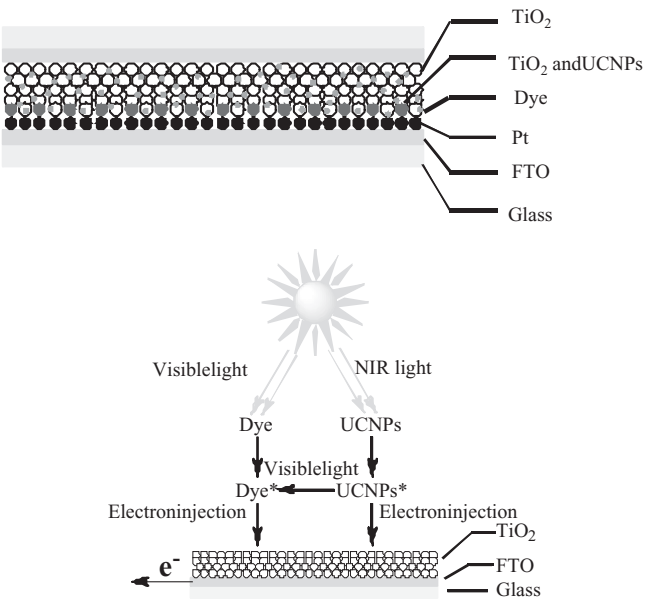

Scheme 1. The structure and working mechanism of UCNP-doped DSCs. FTO = fluorine-doped tin oxide.

nano-heterostructures under AM1.5 G sun. For the device containing TiO_2/$NaYF_4$:Yb^{3+},Ho^{3+} nano-heterostructures, the V_{oc} and the J_{sc} were increased to 0.741 V and 9.00 mA cm^{-2}, and the η reached 4.11%, which is 15% higher than that of the device with photoanode 3 without UCNPs (see Table S2, Supporting Information). The results were similar with those of the device containing TiO_2/$NaYF_4$:Yb^{3+},Er^{3+}. When the nano-heterostructure of TiO_2/$NaYF_4$:Yb^{3+},Tm^{3+} was used, the V_{oc} and the J_{sc} slightly decreased. The effects of the different UCNPs results from the different energy levels of Er^{3+}, Tm^{3+}, and Ho^{3+} (Figure S10, Supporting Information). The green energy levels of Er^{3+} and Ho^{3+} match the CB of TiO_2 well; hence electron transfer could occur easily, and as a result, the photocurrent and overall efficiency of the DSCs with TiO_2/$NaYF_4$:Yb^{3+},Er^{3+} and TiO_2/$NaYF_4$:Yb^{3+},Ho^{3+} nano-heterostructures were obviously increased.

3. Conclusions

We have successfully prepared TiO_2/$NaYF_4$:Yb^{3+},Er^{3+} nano-heterostructures in situ on the TiO_2 photoanode of DSCs. The UCNPs absorbed NIR light and produced an excited electron at a higher energy level (<750 nm); the excited electron can inject directly into the CB of TiO_2. This was confirmed by the up-conversion fluorescence spectrum of the photoanodes containing the nano-heterostructure. The overall efficiency (η) of the DSCs using the photoanodes containing the nano-heterostructure was 17% higher than that of the device without UCNPs and 13% higher than that of the device containing physically mixed TiO_2 and UCNPs, thus highlighting the effect of the direct electron injection from UCNPs to the CB of TiO_2. This result was much better than those in previous works because of the direct electron injection in the nano-heterostructures. Nano-heterostructures of TiO_2/$NaYF_4$:Yb^{3+},Tm^{3+} and TiO_2/$NaYF_4$:Yb^{3+},Ho^{3+} were also prepared in situ on TiO_2 photoanode. The overall efficiency of the device containing TiO_2/$NaYF_4$:Yb^{3+},Ho^{3+} nano-heterostructures was 15% higher than that of the device with photoanode 3, which does not have any UCNPs. When nano-heterostructures of TiO_2/$NaYF_4$:Yb^{3+},Tm^{3+} were used however, the V_{oc} and J_{sc} slightly decreased. The different energy levels of Er^{3+}, Tm^{3+}, and Ho^{3+} results in this different effects caused by the different nano-heterostructures. Our results demonstrate that utilizing the UCNPs with appropriate energy levels can lead to an effective electron injection from the UCNPs to the CB of TiO_2, resulting in an improved photocurrent and overall efficiency for DSCs, all while utilizing NIR light.

Table 1. *I–V* parameters for the control and experimental devices under AM1.5 G filtered spectral illumination at an incident intensity of 100 mW cm^{-2}. J_{sc} = short-circuit current density; V_{oc} = open-circuit voltage; FF = fill factor; Eff = energy conversion efficiency. The results are based on the average of 10 electrodes for each anode material. The effective area of each DSC was 0.36 cm^{-2}.

Sample	V_{oc} [V]	FF	J_{sc} [mA cm^{-2}]	Eff
Photoanode 1	0.765	57.5%	9.47	4.17%
Photoanode 2	0.731	58.4%	8.67	3.70%
Control photoanode 3	0.736	55.8%	8.65	3.55%
Control photoanode 4	0.717	54.8%	8.45	3.32%

4. Experimental Section

Materials: $Y(NO_3)_3{\cdot}6H_2O$ (99.0%), $Yb(NO_3)_3{\cdot}5H_2O$ (99.99%), and $Er(NO_3)_3{\cdot}5H_2O$ (99.9%) were supplied by Aladdin Chemistry Co. Ltd. Analytical grade NaF, ethylene glycol, and oleic acid were purchased from Tianjing Kermel Chemical Reagents Development Center (Tianjing, China). The dye N719, electrolyte, TiO_2 (Degussa product), and platinum electrode were purchased from Dalian HeptaChroma SolarTech Co., Ltd. Ethyl cellulose (M70) and terpinol were supplied by Sinopharm Chemicals Reagents Co., Ltd (Shanghai, China).

Synthesis of $NaYF_4$:Yb,Er Nanocrystals with Small Size: The $NaYF_4$:Yb,Er nanocrystals were synthesized using an improved synthesis relative to the traditional hydrothermal method. An aqueous solution (2.5 mL) of 0.4 M 78% $Y(NO_3)_3$, 20% $Yb(NO_3)_3$, and 2% $Er(NO_3)_3$ was mixed with 1.5 mL of deionized water and 39 mL of ethylene glycol at room temperature with stirring. Afterwards 7 mL of oleic acid were added into the solution, resulting in solution A. NaF (504 g) was dissolved in 10 mL of deionized water to form solution B. After stirring solution A for 0.5 h, solution B was added to solution A dropwise under vigorous stirring. After aging for 30 min, the mixture was transferred to a 76-mL Teflon-lined autoclave, sealed, and heated at 200 °C for 7 h. As the autoclave was allowed to cool to room temperature naturally, precipitates collected within; the resulting solid was washed twice with ethanol and then twice with ethanol combined with deionized water. The products were gathered by centrifugation, and then dried in air at 70 °C for 10 h.

Synthesis of $NaYF_4$:Yb,Er Nanocrystals using the Traditional Hydrothermal Synthesis: In a typical synthesis of hexagonal-phase $NaYF_4$:Yb,Er nanocrystals, 2.5 mL of an aqueous solution of 0.4 M 78% $Y(NO_3)_3$, 20% $Yb(NO_3)_3$, and 2% $Er(NO_3)_3$ were combined with 14 mL of deionized water, 16.5 mL of ethanol, and 0.7 g of NaOH at room temperature with stirring. Aftewards 7 mL of oleic acid were added into above solution, forming solution A. NaF (504 g) was dissolved in 10 mL of deionized water and 10 mL of ethanol to form solution B. After stirring solution A for 0.5 h, solution B was added to solution A dropwise under vigorous stirring. After aging for 30 min, the mixture was transferred to a 76-mL Teflon-lined autoclave, sealed, and heated at 200 °C for 7 h. As the autoclave was allowed to cool to room temperature naturally, precipitates collected within; the resulting solid was washed twice with ethanol and *n*-hexane, and then twice with ethanol and deionized water. The products were gathered by centrifugation, and then dried in air at 70 °C for 10 h.

Preparation of TiO_2 Paste: Ethyl cellulose (2 g) was dissolved in 18 g of ethanol while stirring and heating, forming solution A. A 2-g aliquot of solution A was mixed with 400 mg of TiO_2, 1.6 g of terpinol, 30 mL of ethanol, and some zirmil. The mixture was stirred at 450 rpm for 4 h, and then the zirmil was removed by filtration while the ethanol was removed using a rotary evaporator.

Preparation of TiO_2/UCNP Paste: The preparation of TiO_2/UC paste was similar to that of the TiO_2 paste; however, 60 mg of $NaYF_4$:Yb,Er nanocrystals were added before stirring.

Preparation of TiO_2 Electrodes: TiO_2-based photoanodes were fabricated by the screen-printing method, four-layer of TiO_2 paste were printed onto the FTO glass substrates. After sintering at 450 °C for 30 min and subsequent cooling to 80 °C, the TiO_2 photoanodes were immersed in 0.5 mM of N719 acetonitrile:isopropanol (1:1) solution for 24 h. After the adsorption of the dye, the TiO_2 film was taken out, washed with ethanol, and dried under air.

Preparation of TiO_2/UCNP Electrode: The preparation procedure was the same as that used to prepare the TiO_2 electrodes, except that a layer of TiO_2/UCNPs was screen-printed after the four-layer TiO_2 film.

DSC Devices: The counter-electrode was Pt-deposited FTO-glass. The photoanode and counter electrode were clipped together, and iodine electrolyte was inserted between them.

Characterization: X-ray powder diffraction patterns were measured on a Rigaku D/MAX-2400 with Cu-Ka radiation. Up-conversion fluorescence spectra were recorded on a Hitachi F-7000 fluorescence spectrophotometer under the excitation of a 980-nm diode laser. The morphologies of the samples were observed using field-emission scanning electron microscopy (FE-SEM) with a Nova Nanosem 450. TEM and HR-TEM measurements were carried out on a Tecnai F20 S-TWIN microscope operated at 200 kV. The irradiation source for the photocurrent–voltage (*I*–*V*) measurement was an AM1.5 solar simulator (16S-002, SolarLight Co. Ltd., USA). The incident light intensity was 100 mW cm^{-2} calibrated with a standard Si solar cell. The current–voltage curves were obtained by the linear-sweep voltammetry (LSV) method using an electrochemical workstation (LK9805, Tianjing Lanlike Co., China).

Supporting Information

Supporting Information is available from the Wiley Online Library or from the author.

Acknowledgements

This work was supported by the National Natural Science Fundation of China (21076038, 21276040), the Doctoral Fund of the Ministry of Education of China (20100041120024), and the National Key Technology R&D Program 2011BAE07B08.

Received: April 4, 2013
Revised: May 24, 2013
Published online: June 27, 2013

[1] a) B. O. Regan, M. Grätzel, *Nature* **1991**, *353*, 737; b) M. Grätzel, *Nature* **2001**, *414*, 338; c) J. H. Wu, S. C. Hao, Z. Lan, J. M. Lin, M. L. Huang, Y. F. Huang, P. J. Li, T. Sato, *J. Am. Chem. Soc.* **2008**, *130*, 11568.

[2] a) A. Hagfeldt, G. Boschloo, L. Sun, L. Kloo, H. Pettersson, *Chem. Rev.* **2010**, *110*, 6595;b) Z. Ning, H. Tian, *Chem. Commun.* **2009**, 5483.

[3] M. K. Nazeeruddin, P. Pechy, T. Renouard, S. M. Zakeeruddin, R. Humphry-Baker, P. Comte, P. Liska, L. Cevey, E. Costa, V. Shklover, L. Spiccia, G. B. Deacon, C. A. Bignozzi, M. Grätzel, *J. Am. Chem. Soc.* **2001**, *123*, 1613.

[4] F. Gao, Y. Wang, J. Zhang, D. Shi, M. Wang, R. Humphry-Baker, P. Wang, S. M. Zakeeruddin, M. Grätzel, *Chem. Commun.* **2008**, 2635.

[5] H. Choi, C. Baik, S. O. Kang, J. Ko, M. S. Kang, M. K. Nazeeruddin, M. Grätzel, *Angew. Chem. Int. Ed.* **2008**, *120*, 333.

[6] S. Hwang, J. H. Lee, C. Park, H. Lee, C. Kim, C. Park, M. H. Lee, W. Lee, J. Park, K. Kim, N. G. Park, C. Kim, *Chem. Commun.* **2007**, 4887.

[7] Z. Ning, Y. Fu, H. Tian, *Energy Environ. Sci.* **2010**, *3*, 1170.

[8] T. Trupke, M. A. Green, P. J. Wäurfel, *Appl. Phys.* **2002**, *92*, 4117.

[9] V. Badescu, A. M. Badescu, *Renewable Energy* **2009**, *34*, 1538.

[10] J. de Wild, A. Meijerink, J. K. Rath, W. G. J. H. M. van Sark, R. E. I. Schropp, *Energy Environ. Sci.* **2011**, *4*, 4835.

[11] M. Liu, Yalin Lu, Z. B. Xie, G. M. Chow, *Solar Energy Mater. Solar Cells* **2011**, *95*, 80.

[12] B. Guo, A. Hassane, P. D. George, *ACS Appl. Mater. Interfaces* **2011**, *3*, 3239.

[13] G. B. Shan, G. P. Demopoulos, *Adv. Mater.* **2010**, *22*, 4373.

[14] G. X. Xie, J. M. Lin, J. W. Wu, Z. Lan, Q. H. Li, Y. M. Xiao, G. T. Yue, H. F. Yue, M. L. Huang, *Chin. Sci. Bull.* **2011**, *56*, 97.

[15] A. F. Khan, R. Yadav, P. K. Mukhopadhya, S. Singh, C. Dwivedi, V. h. Dutta, S. Chawla, *J. Nanopart. Res.* **2011**, *13*, 6837.

[16] C. Yuan, G. Chen, P. N. Prasad, T. Y. Ohulchanskyy, Z. Ning, H. Tian, L. Sun, H. Agren, *J. Mater. Chem.* **2012**, *22*, 16709.

[17] H. Zeng, J. Li, J. P. Liu, Z. L. Wang, S. H. Sun, *Nature* **2002**, *420*, 395.

[18] a) C. L. Yan, A. Dadvand, F. Rosei, D. F. Perepichka, *J. Am. Chem. Soc.* **2010**, *132*, 8868; b) J. Chang, Y. Liu, J. Li, S. Wu, W. Niu, S. Zhang, *J. Mater. Chem. C* **2013**, *1*, 1168.

[19] S. Ito, P. Chen, P. Comte, M. K. Nazeeruddin, P. Liska, P. Péchy, M. Grätzel, *Prog. Photovolt.: Res. Appl.* **2007**, *15*, 603.

[20] G. B. Shan, M. P. Andrews, T. Gonzalez, H. Djeghelian, *Mater. Lett.* **2008**, *62*, 4187.

[21] C. H. Han, H. S. Lee, K. Lee, S. D. Han, I. Sing, *Bull. Korean Chem. Soc.* **2009**, *30*, 219.